Biogeochemical modelling of dissolved oxygen in a changing ocean

Oliver Andrews*, Erik Buitenhuis, Corinne Le Quéré, Parvadha Suntharalingam

Tyndall Centre for Climate Change Research, School of Environmental Sciences, University of East Anglia, Norwich, NR4 7TJ, UK, ORCID iD 0000-0002-1921-475X

Keywords: ocean deoxygenation; biogeochemical modelling; climate change

Summary

Secular decreases in dissolved oxygen concentration have been observed within the tropical Oxygen Minimum Zones (OMZs) and at mid- to high latitudes over the last ~ 50 years. Earth System Model (ESM) projections indicate that a reduction in the oxygen inventory of the global ocean, termed ocean deoxygenation, is a likely consequence of on-going anthropogenic warming. Current models are, however, unable to consistently reproduce the observed trends and variability of recent decades, particularly within the established tropical OMZs. Here we conduct a series of targeted hindcast model simulations using a state-of-the-art global ocean biogeochemistry model in order to explore and review biases in model distributions of oceanic oxygen. We show that the largest magnitude of uncertainty is entrained into ocean oxygen response patterns due to model parameterisation of pCO_2-sensitive C:N ratios in carbon fixation and imposed atmospheric forcing data. Inclusion of a pCO_2-sensitive C:N ratio drives historical oxygen depletion within the ocean interior due to increased organic carbon export and subsequent remineralisation. Atmospheric forcing is shown to influence simulated interannual variability in ocean oxygen, particularly due to differences in imposed variability of wind stress and heat fluxes.

1. Introduction

The representation of realistic oxygen fields is an important and active area for ocean biogeochemistry model development (e.g. the Fast Met Office UK Universities Simulator [FAMOUS]; [1]) owing to the ecological importance of dissolved oxygen concentration (hereafter [O_2]) and its sensitivity to climatic perturbation on interannual to millennial timescales [2]. Moreover, despite occupying less than 10 % of the ocean by volume, low oxygen waters could account for up to 50 % of open ocean N_2O production as a consequence of denitrification and increased N_2O yields from nitrification under low-[O_2] conditions [3]. ESMs consistently project a reduction in the oxygen content of the global ocean in response to future anthropogenic climate change [4, 5], but with significant uncertainty in the spatial pattern (or "fingerprint") and magnitude [6, 7]. Therefore, the ability of current models to reproduce the observed dynamics and distribution of ocean [O_2] needs to be scrutinised to understand uncertainties and improve projections [8, 9].

A number of persistent model biases have been identified in the [O_2] fields of ocean biogeochemistry models of differing complexity [9, 10] integrated for the historical period. Most evident is the inability of current models to reproduce the observed distribution and variability of [O_2] at low latitudes, particularly within OMZs such as the eastern tropical Pacific [11]. For example, Ocean Biogeochemistry General Circulation Models (OBGCMs) generally simulate historical [O_2] increases within the tropical thermocline

(e.g. [12, 13]) and an overall contraction of suboxic waters [7] in response to ocean warming. These model responses are contrary to time series data compiled for the eastern tropical OMZs [14], which show marked deoxygenation trends and expansion of low-[O_2] waters over the last ~ 50 years. [15] and [11] also highlight the limited capacity of current ESMs to reproduce the observed climatological distribution of [O_2] in the subsurface. This systematic model bias is entrained into the biogeochemically significant [16] volume censuses of low-[O_2] waters, with models variously both underestimating (e.g. HadGEM2-ES [17]) and overestimating (e.g. MPI-ESM-LR [18]; GFDL-ESM2.1 [19]) hypoxic and suboxic extent within the ocean interior. A range of dynamical and biogeochemical model deficiencies have been invoked to explain the divergence between observed and simulated [O_2] at low latitudes (e.g. [1, 9]). Chief among them is the inability of coarse resolution models to explicitly simulate the mesoscale structures which resupply O_2 into the eastern tropical OMZs (e.g. [20]). Eddy-resolving spatial resolution has been shown to improve representation of [O_2] in the Arabian Sea [21] and eastern tropical Atlantic [10] OMZs via more realistic transport processes in the physical model. However, below eddy-resolving scales, improvements in the representation of [O_2] fields with increasing spatial resolution have been shown to be small (e.g. MPI-ESM [18]). Uncertainties surrounding the parameterisation of lateral [22, 15] and vertical [23] diffusion have also been shown to place important constraints on the extent of low-[O_2] waters in coarse resolution ESMs. In addition, unforced variability in the equatorial trade winds has been shown to influence the simulated evolution of tropical OMZs on multidecadal timescales [24], further complicating model-data agreement in coupled models.

The representation of biological processes and their response to physical and geochemical forcing has been suggested as an important limitation on O_2 dynamics in ocean biogeochemistry models (e.g. [25, 26]). For example, [27] show, using an ensemble of ESM experiments, that the interactive effects of climate change and ocean acidification could drive significant alteration to biogeochemical cycles, suggesting that ocean warming should not be considered in isolation when considering future ocean deoxygenation. The potential impacts of ocean acidification on primary and export production are particularly important for oxygen cycling. Mesocosm experiments carried out using natural plankton communities [28, 29] suggest that the C:N uptake ratio in photosynthetic carbon fixation increases under elevated pCO_2 due to DIC over-consumption, causing the composition of exported organic material to deviate from classical Redfield stoichiometry (e.g. C:N = 6.6 [30]). Specifically, [28] report higher C:N drawdown ratios in diatom and coccolithophore-dominated mesocosm enclosures exposed to increased partial pressures of CO_2 (pCO_2 = 700 μatm, C:N = 7.1; pCO_2 = 1050 μatm, C:N = 8.0), whilst N:P ratios remain unchanged from Redfield proportions. The effects of stoichiometric plasticity in marine ecosystems remain largely unaccounted for in current ocean biogeochemistry models [31], which generally rely on fixed elemental ratios in the formation of organic material. However, studies using configurations of the UVic [32] and PISCES [33] models which implement a pCO_2 sensitive C:N ratio in primary production suggest that stoichiometric effects in response to ocean acidification could have a major impact on biogeochemical cycles. Model experiments with variable C:N stoichiometry simulate increases in cumulative carbon export of between 70 and 100 Pg C by 2100 in response to future CO_2 forcing. Moreover, the export of (relatively) more carbonaceous organic material from the surface in response to DIC over-consumption driven by acidification also causes biological oxygen demand to increase. As a result, these model experiments project elevated deoxygenation of the tropical thermocline (> 20 μmol L^{-1}) and 36 – 50% increases in the volume of suboxic waters by 2100 [32, 33], compared to no change or a small [O_2] increase as simulated by fixed stoichiometry ESMs [6]. [9] investigate the impact of variable C:N ratios on historical [O_2] trends using an intermediate complexity ESM, and find that this effect is small for zonal mean [O_2] trends at 300 dbar. However, the impact of accounting for variable stoichiometry on historical [O_2] changes in more complex Plankton Functional Type (PFT) ocean biogeochemistry models (e.g. [34, 35]) remains uncertain.

Another potentially important impact of biological processes on [O_2] changes relates to the well-established [36] effect of ocean acidification on the saturation state of seawater with respect to calcium

carbonate (both calcite [Ω_{cal}] and its less stable polymorph aragonite [Ω_{arag}]). A decrease in Ω under elevated pCO_2 has been shown by a number of laboratory and field studies to reduce biogenic calcification rates in some calcareous holoplankton (foraminifera, pteropods and some coccolithophores) and warm-water corals [37]. Extrapolating these results, [38] projects a ~ 50 % decline in global $CaCO_3$ export production by 2250 using an OBGCM which accounts for reduced biocalcification rates in response to ocean acidification (SRES A1B emissions scenario). Beyond direct effects, it has been suggested by [39] that changes in the "carbonate pump" may also impact upon the export of organic material, since fluxes of POC and PIC are highly correlated beneath ~ 1000 m depth (the so-called "PIC:POC rain ratio" [40, 41]). Specifically, export fluxes of dense calcareous ($CaCO_3$) and siliceous (SiO_2) biominerals provide ballast which increases the sinking speed and transfer efficiency of POC into the ocean interior. Therefore, reduced export production of $CaCO_3$ in response to ocean acidification could impact upon the efficiency of the organic ("soft tissue") biological pump, such that POC remineralises at shallower depths as mineral ballast fluxes weaken. This effect has been reproduced by OBGCMs which include simple ballasting sub-models [38], with implications for other biogeochemical cycles including oxygen. For example, [42] demonstrated, using idealised experiments with a [CO_3^{2-}] dependency in calcification rates (R_{CAL}), that shallower POC remineralisation depths in response to weakened ballasting exacerbates O_2 depletion within established subsurface [O_2] minima. Specifically, reduced ballasting alone is shown in prognostic experiments under a SRES A1F1 emissions scenario until 2100 (with emissions declining to 0 at 2200) to reduce [O_2] by 20 – 40 μmol L^{-1} between ~ 200 – 800 m depth by the year 3000, with the largest decreases within tropical OMZs (e.g. > 50 μmol L^{-1} at 500 m depth in the Arabian Sea). Thus, the effects of ocean acidification on carbon export have been shown to have a major impact on [O_2] distributions and forced responses in model projections. However, no studies have so far addressed if these missing processes could reconcile the mismatch between observed and modelled [O_2].

Current ocean biogeochemistry models also generally underestimate temporal variability in O_2 on interannual to decadal timescales. For example, [43, 44] report decadal scale variability in Apparent Oxygen Utilisation (AOU) as simulated by an ensemble of ocean-only hindcast model experiments for the North Pacific region to be underestimated by a factor of ~ 3 relative to repeat hydrographic section data. Similarly, interannual variability in global Atmospheric Potential Oxygen fluxes have been shown to be underestimated by a factor of ~ 2 - 4 in hindcast ocean biogeochemistry models relative to those estimated using global atmospheric transport inversions [26]. These results are also consistent with the model-data comparison of [8], where optimal detection methods applied to Coupled Model Intercomparison Project Phase 5 (CMIP5) ESMs show that model [O_2] responses need to be scaled up by a factor of ~ 2 – 4 to match observed changes. Recent work using hindcast models [45, 46, 47] demonstrate the sensitivity of simulated trends and variability in the ocean carbon cycle to imposed atmospheric forcing. For instance, [47] find significant differences in the interannual variability of CO_2 outgassing fluxes from the tropical Pacific using ocean-only OBGCM experiments forced with the JPL CCMP Ocean Surface Wind Product [48] compared to NCEP/NCAR reanalysis data [49]. Additionally, model representation of large scale physical transport processes such as the Atlantic Meridional Overturning Circulation (AMOC) have been shown to be sensitive to the choice of imposed atmospheric forcing. For example, [50] show model simulated long period variability in AMOC transport at 26.5°N to be significantly different between hindcast experiments which employ ECMWF ERAInterim reanalysis data [51] compared to those which calculate bulk fluxes using the Drakkar Forcing Set 3 (DFS3; [52]) blended meteorological and satellite forcing product. As a result, whilst it must be acknowledged that natural variability is also generated internally to the ocean system, ocean-only model configurations allow considerable "exogenous" variability to be directly related to the imposed atmospheric forcing. Therefore, the use of high frequency, high quality atmospheric data to calculate turbulent fluxes of heat, freshwater and momentum in hindcast models (cf. [52, 53]) could provide a mechanism for improving interannual to decadal variability in simulated O_2.

The present study explores the source of systematic biases in model representation of [O_2] with a range of physical and biogeochemical perturbation experiments conducted using a state-of-the-art global ocean biogeochemistry model. It focuses on quantifying the impact of (a) ocean acidification (variable C:N

stoichiometry and mineral ballasting) and (b) imposed atmospheric forcing on the spatiotemporal distribution of [O_2] over the last ~ 50 years.

2. Model description

(a) Ocean biogeochemistry model

PlankTOM10 is a global ocean biogeochemistry model which describes lower-trophic level ecosystem dynamics explicitly based on PFTs [35, 54, 55]. It includes ten PFTs: picophytoplankton, N_2-fixers, coccolithophores, mixed phytoplankton, diatoms, colonial *Phaeocystis*, bacteria, protozooplankton, mesozooplankton and macrozooplankton. The present model version, fully documented in [35], comprises 39 biogeochemical tracers, and simulates the full marine cycles of Carbon (C), Phosphorous (P), Oxygen (O_2), Silicon (Si), along with simplified cycles of Nitrogen (N) and Iron (Fe). Growth of PFTs is co-limited by temperature, light, macronutrients (N, P and Si) and Fe. PlankTOM10 includes 3 detrital pools (semi-labile dissolved organic material [DOM], and small and large POC), with a fixed Redfield stoichiometry (172O : 122C : 16N : 1P [56]) in the formation and remineralisation of organic material for the standard model configuration. Ratios for Fe : C, Chl : C and Si : C (for diatoms) of organic material are variable, calculated by the model based on PFT and abiotic factors [34]. N pools are also subject to denitrification and N_2-fixation processes. PlankTOM10 also includes mineral ballasting, whereby the sinking speed of large POC increases as a function of opal (SiO_2) and calcite ($CaCO_3$) content. This parameterisation applies the direct measurements of mineral ballasting by opal and calcite in copepod fecal pellets [57] to the drag equations [58]. The drag equations are solved offline by iteration in order to calculate gravitational sinking speeds of large POC (v_{sink}) over the range of particle densities in the model. These pairs of particle densities and sinking speeds could be well represented by the following equation (2.1).

$$v_{sink} = a \times (\rho_{par} - \rho_{sw})^b \qquad (2.1)$$

where a = 0.0303, b = 0.6923, ρ_{sw} is the density of seawater and ρ_{par} is the density of the particle, calculated by:

$$\rho_{par} = \frac{(POC \times 240 + CAL \times 100 + SIL \times 60)}{POC \times \left(\frac{POC \times 240}{\rho_{POC}} + \frac{CAL \times 100}{\rho_{CAL}} + \frac{SIL \times 60}{\rho_{SIL}} + \rho_{sw}\right)} \qquad (2.2)$$

where *LPOC* is large particulate organic carbon, *CAL* is sinking calcite, *SIL* is sinking opal, 240 is wet weight/mol POC, 100 is the molar mass of calcite, 60 is the molar mass of opal, and ρ_{LPOC} = 1.08 kg L^{-1}, ρ_{CAL} = 1.34 kg L^{-1}, ρ_{SIL} = 1.2 kg L^{-1} (calculated based on the data of [57]). Small POC is set to sink at a constant rate of 3 m d^{-1}, whereas *LPOC* has a maximum numerically stable sinking speed set to 150 m d^{-1}.

Biogeochemical fields are initialised from observations of the Global Ocean Data Analysis Project (GLODAP; [59]) data for Dissolved Inorganic Carbon (DIC) and alkalinity, and World Ocean Atlas 2005 for O_2 [60] and nutrients [61]. Biological variables are initialised as in [62], with initial concentrations available at http://opendap.uea.ac.uk:8080/opendap/greenocean/Restart/. As described in [35], PFTs were not impacted by initialisation and equilibrated within 3 years of model integration.. The model is forced with atmospheric CO_2 concentration at each timestep [63]. Dust fluxes are interpolated to daily values from the monthly fields of [64], providing surface Fe and Si inputs.

(b) Physical model

PlankTOM10 is embedded within the Nucleus for European Modelling of the Ocean version 3.1 (NEMOv3.1) physical model, which comprises the primitive equation Océan Parallélisé version 9 (OPA9; [65]) ocean GCM coupled to the Louvain–la–Neuve Ice version 2 (LIM2; [66]) dynamic-thermodynamic sea ice model. This study employs a global configuration (ORCA2; [67]) of NEMOv3.1 where the model is discretised on a tripolar curvilinear grid with a zonal resolution of 2°, and a meridional resolution of 2° × cos(latitude) increasing to ~ 0.5° at the equator and towards the poles. In the vertical, ORCA2 has 30 z-levels with a maximum resolution of 10 m for the upper 100 m, decreasing to ~ 500 m at 5 km depth. Vertical mixing is calculated using a turbulent kinetic energy model [68], with subgrid scale eddy-induced mixing processes accounted for using the parameterisation of [69]. Active tracers are initialised from World Ocean Atlas 2005 temperature [70] and salinity [71] observations. A range of atmospheric forcing data has been used to derive surface fluxes of momentum, heat and freshwater as boundary conditions to the hindcast model, as described in Section 3b.

3. Simulation set-up

As outlined in Table 1, ocean biogeochemistry (Sect. 3a) and atmospheric forcing (Sect. 3b) sensitivity experiments are carried out using the PlankTOM10-NEMOv3.1 model to explore and review impacts on simulated historical distributions of [O_2]. In order to isolate the impact of perturbations, model fields are generally presented relative to a baseline reference configuration. This approach is consistent with other model studies which evaluate the impact of incorporating new processes [72] or anthropogenic impacts [73] via comparison with an unperturbed experiment. As a result, non-equilibrium artefacts and other dynamical processes are removed, such that this analysis focuses on understanding the impact of these imposed changes on hindcast biogeochemical tracers. This work therefore presents a synthesis of sensitivity experiments, and differs from other studies (e.g. [9]) focusing on model-data comparison of absolute changes in [O_2] over the historical period. This established approach [e.g. 46] allows for representation of trends and variability in a "process-level" model study to be improved due to the relatively short hindcast period over which observed vertical gradients in [O_2] are preserved.

Results from ocean acidification experiments are presented averaged over the period 2003 – 2013 (Sect. 4a), allowing for the largest adjustments to initial conditions to occur over the first ~ 50 model years. De-trended results from the ensemble of atmospheric forcing experiments are presented over their common time period (1958 – 2005) to avoid sampling biases associated with differing temporal ranges (Sect. 4b).

(a) Ocean acidification experiments

Two biogeochemistry perturbation experiments are conducted over the historical period to investigate the impact of ocean acidification on the spatiotemporal distribution of [O_2], alongside a baseline (*REF*) experiment following the standard model configuration. These comprise explicit representation within PlankTOM10 of (1) a pCO_2 sensitive C:N ratio in primary production (*STO10*) and (2) a pCO_2 sensitive calcification rate (R_{CAL}) and associated impacts on the PIC:POC rain ratio (*BAL10*). Ocean biogeochemistry experiments are conducted using a common atmospheric forcing (*REF*; Sect. 3b).

For the *STO10* experiment, a change in the C:N ratio of organic matter via increased photosynthetic carbon fixation in response to ocean acidification is parameterised using the results of mesocosm experiments carried out on natural plankton communities under elevated pCO_2 [28]. A non-dimensional "CO_2-sensitivity" factor is used to provide a relationship between pCO_2 model forcing and the C:N ratio in simulated organic carbon production and remineralisation. Following the prognostic model study of [32], a linear relationship between imposed pCO_2 and C:N is derived based upon the results of [28] for measured C:N values provided at pCO_2 values of 350 μatm, 700 μatm, and 1050 μatm. Also following [32], this CO_2-sensitivity factor is re-scaled back to an assumed pre-industrial pCO_2 of 280 ppm which increases the C:N for a given pCO_2, therefore our estimate provides an upper bound for this overconsumption effect

over the historical period. In *STO10* this factor is multiplied by the rate of net organic carbon production and used to calculate a variable (pCO_2-sensitive) O:C ratio in organic material. Variable C:N ratios in organic material are linked to imposed atmospheric pCO_2 rather than surface water pCO_2, enabling direct comparison with a fixed C:N ratio *REF* experiment. In support of this, [32] show that simulated changes in $[O_2]$ over longer (centennial) timescales are insensitive to this distinction.

For the *BAL10* experiment, the impact of a pCO_2 sensitive biogenic calcification rate (R_{CAL}) on marine biogeochemical cycles is parameterised using results from laboratory manipulations carried out with coccolithophore species, in which the PIC:POC rain ratio is measured to decrease under elevated $[CO_{2(aq)}]$ [74]. PlankTOM10 includes explicit representation of coccolithophores as a calcifying PFT with growth rates based on observations. Thus, the experimentally-derived parameterisation can be applied directly to coccolithophore responses rather than more generically. Following [74] and [38], the $CaCO_3$:C_{ORG} production ratio ($R_{CaCO3/Corg}$) is parameterised in *BAL10* as a function of pCO_2:

$$\mathbf{!}^{\mathbf{!"!\#!/!!"\#}} = \mathbf{!}^{\mathbf{!"!\#!/!!"\#}} \cdot \left(1 - \mathbf{!} \cdot \left(\mathbf{!}^{\mathbf{!"\#}} - \mathbf{!}^{\mathbf{!"\#}}\right)\right) \qquad (3.1)$$

where A = 4.4 x 10^{-4} (based on [74]), pCO_2^{preind} = 277.32 ppm and pCO_2^{obs} is prescribed from observations [63].

(b) Atmospheric forcing experiments

Gridded atmospheric data are used to prescribe surface boundary conditions to ocean models. In this study, a series of model experiments are conducted using different atmospheric data to investigate the sensitivity of variability in simulated ocean $[O_2]$ to imposed forcing. Simulations are carried out using four different atmospheric forcing data products (Table 2). These experiments also differ in terms of the bulk formulae used to provide turbulent fluxes of momentum, heat and freshwater to the physical ocean model.

As summarised in Table 2, the baseline *REF* experiment uses a CLIO bulk formulation [75] to calculate surface boundary conditions from daily frequency NCEP/NCAR 10 m air temperature (θ_{10}), 10 m u and v wind components (U_{10}, V_{10}), total precipitation rate (*pptn*), 10 m specific humidity (q_{10}) and total cloud cover (*tcdc*). Three other experiments (*CORE2*, *DFS4*, *IPSL*) are conducted, all of which employ a more recent bulk formulation (CORE; [53, 76]), which requires a slightly different set of surface variables, including downwelling shortwave (rad_{sw}) and longwave (rad_{lw}) radiation and precipitation as a total precipitation rate (*precip*) and solid fraction (*snow*).

CORE2 is forced with Version 2 of the Common Ocean-Ice Reference Experiments Inter-annually Varying Forcing (COREv2-IAF) dataset [53, 76]. COREv2-IAF is a hybrid forcing product, which applies corrections to known biases in NCEP/NCAR reanalysis state variables (U_{10}, V_{10}, θ_{10}, q_{10}) and utilises satellite derived radiative flux (ISCCP-FD [77]) and precipitation (merged GCGCS product [76]) estimates so as to limit the imbalance in model heat and freshwater budgets.

DFS4 is forced with the DRAKKAR Atmospheric Forcing Set Version 4.3 (DFS4.3 [52]) data. Following the COREv2-IAF approach, DFS4.3 is also a hybrid forcing product using satellite radiation (ISCCP-FD) and precipitation (GCGCS). Surface atmospheric state variables are, however, provided from ERA-40 ECMWF reanalysis data [78], with adjustments as described in [52]. ERA-40 is considered a "second generation" reanalysis product, with improvements in terms of resolution, data assimilation methods, and atmospheric models.

IPSL is forced with model data generated from the output of a CMIP5 ESM. Historical integrations of the IPSL-CM5A-LR ESM [79] were conducted under CMIP5 (1850 – 2005) with climatic forcings prescribed

from observations [80]. Here, output from one ensemble member of the "historical" experiments (*r1i1p1*) was processed to extract atmospheric data according to the approach of *DFS4* and *CORE2*, however temporal frequency was limited by the availability of model output. Thus, daily frequency U_{10}, V_{10}, θ_2, q_2, rad_{sw} and rad_{lw} were used along with monthly mean *precip* and *snow*, with modifications made to the physical model set-up to account for changes in temporal frequency. IPSL-CM5A-LR ESM was selected in order to limit the physical inconsistency with PlankTOM10-NEMOv3.1, since IPSL-CM5A-LR also utilises the NEMO physical model, whilst also reducing errors associated with spatial interpolation. Other studies have conducted prognostic ocean-only OBGCM experiments using CMIP5 atmospheric data (e.g. [81]), however the impact of an ESM-derived forcing in hindcast model configurations remains underanalysed.

4. Results

(a) Ocean acidification experiments

For *STO10*, the effects of ocean acidification on the C:N ratio of organic carbon production drives changes to simulated POC export from the euphotic zone (Fig. 1a) and DIC distribution (Fig. 1b – 1c). Globally, POC export at 100 m is higher by more than 0.2 mol C m^{-2} y^{-1} relative to the fixed C:N ratio *REF* experiment, corresponding to a ~ 20 % area mean increase. The higher POC export is most pronounced (> 0.3 mol C m^{-2} y^{-1}) within established high-production regions of the global ocean, such as the eastern boundary upwelling system of the equatorial Pacific (Fig. 1a). Comparable increases in export are also found at mid- to high-latitudes (40 – 60°) within the subpolar North Pacific, North Atlantic and Southern Ocean, where existing high rates of annual primary production associated with the spring blooms are accentuated. In contrast, POC export fluxes show a smaller increase within the mid-latitude oligotrophic gyres, however this corresponds to a similar relative increase (15 – 20 %) when compared to more productive regions. Coeval historical decreases in DIC at 100 m depth across much of the tropical and mid-latitude ocean (up to 3 μmol L^{-1}) are consistent with carbon overconsumption within the euphotic zone in response to the CO_2 fertilisation (Fig. 1b). Lower DIC concentrations ([DIC]) simulated within the euphotic zone are opposed by zonal mean [DIC] increases (> 5 μmol L^{-1}) at depth, associated with a strengthened "soft tissue" pump as more exported POC is remineralised (Fig. 1c). Elevated remineralisation driven alteration to the DIC profile at intermediate depths is associated with high POC sinking speeds and model underestimation of upper ocean bacterial biomass (0 – 200 m; [35]).

For *BAL10*, the global mean ratio of $CaCO_3$ to POC export production (EXP_{CaCO3}/EXP_{POC}) at 100 m decreases by 4.9 % relative to *REF*, consistent with a reduced rate of biogenic calcification in response to ocean acidification. The largest decreases in EXP_{CaCO3}/EXP_{POC} occur within the tropical Indian Ocean and eastern tropical Atlantic Ocean, and in mid- to high-latitude regions of the North Atlantic and North Pacific (Fig. 2a). Reductions in EXP_{CaCO3}/EXP_{POC} of up to ~ 0.01 are similar in magnitude to those reported by [42] in [CO_3^{2-}]-sensitive R_{CAL} experiments for 2003 – 2013. Within the North Pacific, marked decreases in EXP_{CaCO3}/EXP_{POC} are centered on the North Pacific Current (NPC) region. The eastward flowing NPC is a major transverse surface current which bisects the subtropical and subarctic North Pacific and plays an important role in the resupply of nutrients and oxygen into the interior of the Alaskan gyre [82], where secular [O_2] decreases have been observed [83]. Thus, EXP_{CaCO3}/EXP_{POC} reductions in the NPC could have important downstream implications for biogeochemical cycles in the eastern subpolar North Pacific and California Current region [84].

In *BAL10*, reduced export of $CaCO_3$ mineral ballast from the surface ocean causes a global mean reduction in model simulated gravitational sinking speeds for large POC (*vsink*) between 0 – 2000 m depth of 0.2 m d^{-1} (0.4 %). The spatial pattern of *vsink* reductions is most pronounced (> 0.5 m d^{-1}) where EXP_{CaCO3}/EXP_{POC} decreases are largest (Fig. 2b). As such, perturbation to the PIC : POC "rain ratio" can be invoked to explain coeval changes in sinking speeds of large POC.

Changes in the carbon cycle impact upon the spatiotemporal distribution of [O_2] in *STO10* via changes to the rate of oxygen production and consumption. Mirroring the pattern of DIC concentration changes (Fig. 1c), zonal mean [O_2] in *STO10* increases by up to 6 μmol L^{-1} within the more productive (sub)tropical euphotic zone (Fig. 3a). These near-surface [O_2] increases are opposed by marked deoxygenation throughout much of the ocean interior, particularly at mid- to high- latitudes, where biological oxygen demand rises as more carbonaceous (> C:N ratio) organic material is remineralised at depth. Subsurface [O_2] depletion reaches a zonal mean maximum of > 10 μmol L^{-1} within intermediate waters of the subpolar North Atlantic (~ 60°N). The signature of depth-averaged zonal mean [O_2] change scales with latitude, such that the largest [O_2] decreases (≥ 2 μmol L^{-1}) occur poleward of 60° in regions of deep water renewal. As such, the inclusion of acidification effects in organic carbon production could act to augment the historical fingerprint of climate-driven ocean deoxygenation produced by fixed stoichiometry models [6].

The inclusion of a variable C:N ratio in carbon fixation in *STO10* also impacts upon the characteristics of simulated low-[O_2] waters. Decreases in minimum [O_2] values are most pronounced (> 8 μmol L^{-1}) within the subpolar North Atlantic, and for the Indian Ocean and eastern equatorial Pacific OMZs (not shown). Associated with this intensification of low-[O_2] conditions, *STO10* simulates an increase in the number of suboxic (+ 2 %, [O_2] ≤ 5 μmol L^{-1}) and hypoxic (13 %, [O_2] ≤ 60 μmol L^{-1}) grid cells, relative to *REF*. Expansion of low-[O_2] waters also impacts upon nitrogen cycling, with the promotion of denitrification processes under suboxic conditions where nitrate is used as an oxidant in the remineralisation of organic material. Global area mean denitrification rates increase by 0.27 μmol N m^{-3} y^{-1} (34 %, 0 – 2000 m), associated with oxygen depletion in response to elevated POC export fluxes.

Compared with *STO10*, changes in the carbon cycle associated with *BAL10* cause almost no change in zonal mean [O_2] relative to *REF* (Fig. 3b). However, in agreement with the prognostic model results of [42], *BAL10* reproduces a small [O_2] decrease relative to *REF* within the ventilated thermocline (100 – 1000 m), which is likely to be exacerbated in response to future pCO_2 forcing. Aside from imposed pCO_2, the more muted magnitude of [O_2] change simulated by *BAL10* can also be attributed to the relatively small overall global export production which dampens the impact of any acidification driven reductions in EXP_{CaCO3} on EXP_{CaCO3}/EXP_{POC}. However, generally the results of *BAL10* suggest that the inclusion of a pCO_2-sensitive biocalcification rate in an ocean biogeochemistry model does not impact significantly upon simulated O_2 dynamics for the historical period, despite alteration to EXP_{CaCO3}/EXP_{POC} and sinking speeds of large POC.

(b) Atmospheric forcing experiments

Simulated standard deviation in annual mean thermocline (300 m) [O_2] is presented as a metric of interannual variability following other model studies which assess the bulk variability properties of upper ocean O_2 using either a ~ 300 m depth interval [85] or surface fluxes [25, 86]. Variability differs between model experiments (Fig. 4), with *DFS4* exhibiting the largest area mean variability ($\sigma_{[O2]}$ = 2.4 μmol L^{-1}) when compared to *CORE* ($\sigma_{[O2]}$ = 1.9 μmol L^{-1}) and *IPSL* ($\sigma_{[O2]}$ = 1.8 μmol L^{-1}). Differences in temporal frequency of input forcing data used for the *IPSL* CORE experiment (Table 2) are found to have only a small impact on simulated $\boldsymbol{\sigma_{[O2]}}$ (2 % change in area mean $\sigma_{[O2]}$) in sensitivity analyses carried out with *DFS4* at the temporal frequency of *IPSL* (Fig. S1). Elevated $\sigma_{[O2]}$ in the DFS4.3 experiment suggests that ERA-40 derived forcing products generate more exogenous variability in passive tracer fields of ocean-only models when compared to NCEP/NCAR (*REF*, *CORE2*) based atmospheric data. However, a number of other differences between forcing products (Table 2) could also contribute to the larger interannual variability in *DFS4*, for instance the alteration to surface fluxes caused by referencing of DFS4.3 surface air temperature and specific humidity at 2 m rather than 10 m.

[O_2] fields are also taken from biogeochemical output of the IPSL-CM5A-LR CMIP5 "historical" experiment (*ESM*; Fig. 4e) used to derive the atmospheric forcing for *IPSL*. As a result, direct comparison can be drawn between variability in the coupled IPSL-CM5A-LR ESM configuration and the ocean-only PlankTOM10-NEMOv3.1 experiment conducted using atmospheric fields from this integration. The coupled IPSL-CM5A-LR model (*ESM*) simulates more variability in thermocline [O_2] (area mean $\sigma_{[O2]}$ = 2.7 μmol L^{-1}) relative to the ensemble mean of all ocean-only atmospheric forcing experiments ($\sigma_{[O2]}$ = 2.1 μmol L^{-1}). Since *IPSL* and *ESM* experiments include identical atmospheric forcings along with similar physical and biogeochemical model components (*IPSL* = PlankTOM10-NEMOv3.1; *ESM* = PISCES-NEMOv3.2 [79]) the residual interannual variability between experiments ($\sigma_{[O2]}^{ESM-IPSL}$ = ~ 1 μmol L^{-1}) can plausibly be attributed to that which is generated internally to the ocean-atmosphere system under a coupled formulation.

Simulated interannual variability scales with latitude for all model experiments, such that $\sigma_{[O2]}$ is most pronounced ($\sigma \geq 4$ μmol L^{-1}) poleward of 40° in both hemispheres. All model experiments exhibit an elevated $\sigma_{[O2]}$ signal of up to 10 μmol L^{-1} within the north-western subpolar gyre of the North Atlantic and subpolar central and western North Pacific (Fig. 4). These regional patterns have been identified in other O_2 modelling studies (e.g. [25, 85]) and are associated with the NAO and PDO, respectively, which provide the dominant source of Northern Hemisphere climate variability on interannual to decadal timescales. All experiments converge on a maximum $\sigma_{[O2]}$ of ~ 6 μmol L^{-1} at ~ 60°N consistent with variability associated with the dominant climate modes, whereas the signal of interannual variability in the Southern Ocean is less certain – with zonal mean $\sigma_{[O2]}$ ranging from 1 – 7 μmol L^{-1} for different atmospheric forcings south of 60°S (Fig. 4f). Particularly, the *CORE2* and *IPSL* experiments simulate $\sigma[O_2] \leq 2$ μmol L^{-1} across much of the Southern Ocean whereas zonal mean $\sigma[O_2]$ exceeds 4 μmol L^{-1} for *REF*, *DFS4* and *ESM* (Fig. 4f).

Interannual variability in windspeed (σ_{wspd}; Fig. 5a) and near-surface air temperature (σ_θ; Fig. 5b) also differ between imposed atmospheric forcing products. DFS4.3 exhibits the largest zonal mean variability in windspeed and near-surface air temperature, consistent with the largest simulated $\sigma_{[O2]}$ of all ocean-only experiments (Fig. 4c). However, DFS4.3 windspeed and near-surface air temperature data do not reproduce the meridional structure of σ_{wspd} and σ_θ exhibited by all other forcing fields. Excluding DFS4.3, the largest inter-forcing divergence in σ_{wspd} occurs in the tropics (20°S – 20°N) where elevated interannual variability in COREv2-IAF tropical windspeeds (~ 0.5 m s^{-1}) relative to IPSL-CM5A-LR derived winds (~ 0.25 m s^{-1}) can be invoked to explain the more muted tropical variability in thermocline [O_2] ($\sigma_{[O2]}$) of *IPSL* compared to *CORE2* (Fig. 4f). In contrast, larger interannual variability in σ_{wspd} does not generate a first-order response in $\sigma_{[O2]}$ at mid- to high-latitudes, with, for example, elevated variance in the westerlies over the Southern Ocean for *IPSL* not being associated with a coeval increase in $\sigma_{[O2]}$ (Fig. 4d).

The largest deviation in zonal mean σ_θ between atmospheric datasets occurs poleward of 60°S, where COREv2-IAF exhibits lower interannual variability (σ_θ = ~ 0.4 K) when compared to IPSL-CM5A-LR (σ_θ = ~ 0.8 K) and NCEP/NCAR reanalysis (σ_θ = ~ 1.2 K) derived near-surface air temperatures. These σ_θ differences track the inter-experiment divergence in $\sigma_{[O2]}$ for the Southern Ocean, such that model biases in the simulation of thermocline [O_2] variability agree with differences in the magnitude of imposed σ_θ. Specifically, reduced interannual variability in near-surface air temperature in *CORE2* and *IPSL* can be related to lower $\sigma_{[O2]}$ relative to *REF*, which exhibits elevated σ_θ and, therefore, $\sigma_{[O2]}$ poleward of 60°S. This modulation of tropical O_2 variability by windspeed and extratropical (subpolar) O_2 variability by surface heat flux has been reproduced by other forced ocean biogeochemistry models investigating variability in North Atlantic O_2 fluxes [86].

5. Discussion and summary

To date, much research has focused on understanding the impact of biogeochemical [27, 32, 33] and physical [6, 7] processes in OBGCMs on simulated future climate-driven perturbation to the global oxygen inventory. This work, rather, aims to better constrain the implications of the interrelated physical-

biogeochemical drivers for [O_2] dynamics over the historical period, towards reconciling the well-documented [9] discrepancies between model-simulated and observed [O_2] changes. As highlighted by [2], a "critical first step" in our understanding of oxygen dynamics in a warming world is the development of models at regional and global scales with the capacity to reproduce observed trends and variability. Accordingly, continued efforts to improve model-data agreement in [O_2] at the process level are required, in order to gain a mechanistic understanding of observed changes in oceanic oxygen towards improved predictions of future change. To this end, model experiments conducted here reveal that the sign and magnitude of [O_2] change over the last ~ 50 years depend critically on ocean acidification feedbacks and prescribed air-sea fluxes of heat, water and momentum.

Our results suggest that explicit representation of observationally-based ocean acidification impacts on photosynthetic carbon drawdown yields major changes to the spatiotemporal distribution of simulated POC export and, consequently, subsurface O_2 utilisation. Historical POC export changes associated with the inclusion of a pCO_2-sensitive C:N ratio are similar in magnitude but differ in sign to the absolute historical changes predicted by current fixed stoichiometry models as a result of secular ocean warming. For example, [87] report POC export at 100 m decreases by ~ 0.5 mol C m^{-2} y^{-1} for much of the extrapolar ocean between 1960 and 2006 in hindcast simulations of the CCSM3-BEC model. With the inclusion of a pCO_2-sensitive C:N ratio, POC export at 100 m increases by > 0.3 mol C m^{-2} y^{-1}, suggesting that stoichiometric effects could act to compensate a significant component of the "direct" climate-driven reduction in export production. Thus, as highlighted by [33] the inclusion of stoichiometric plasticity in the next generation of ESMs could alter the classical view that historical [87] and future [88] anthropogenic forcing drives a simulated reduction in global marine production, the observational basis for which remains contested [89, 90]. Equally, [87] report increases in POC export of up to 0.6 mol C m^{-2} y^{-1} in subpolar (light-limited) regimes, associated with historical density stratification increases in their hindcast model. In this case, the inclusion of ocean acidification effects on organic carbon drawdown could act to amplify secular increases in POC export change associated with ocean warming. Development of high complexity ocean biogeochemistry models which dynamically resolve stoichiometry (e.g. ERSEM [91]) provide a framework for investigating diverse ecosystem responses to changes in environmental conditions.

A strengthened "soft tissue" pump associated with the inclusion of a pCO_2-sensitive C:N ratio also drives major changes to simulated remineralisation within the ocean interior, as evidenced by stronger gradients in [DIC] and [O_2]. Coeval subsurface [O_2] decreases and a reduction to the global inventory of O_2 are consistent with model projections which include pCO_2-sensitive C:N ratios in carbon fixation (e.g. [32, 33]). However, counter to published model experiments, the spatial pattern of [O_2] decrease associated with carbon overconsumption in this study follows the absolute fingerprint of (observed) ventilation-driven deoxygenation (see [92]), with the most pronounced O_2 depletion occurring at mid- to high- latitudes, rather than focused within the tropical OMZs. This result does not, therefore, support the suggestion (e.g. [4]) that inclusion of a pCO_2-sensitive C:N ratio in carbon fixation could invoke a net deoxygenation of the tropical thermocline for the historical period, in agreement with recent hindcast [9] and prognostic [27] ESM experiments which include variable stoichiometry. Rather, stoichiometric effects in response to historical ocean acidification are shown here to bring about elevated oxygen depletion in mid- to high latitude regions of water renewal, thus providing a biogeochemical amplifier for (chiefly) physically driven simulated [O_2] changes (e.g. [6]). Accordingly, the inclusion of these effects in the next generation of ESMs could act to reduce the discrepancy between observed [91] and more muted ESM simulated historical deoxygenation trends. Additionally, consistent with prognostic model studies, the inclusion of a pCO_2-sensitive C:N ratio here produces an increase in the modelled volume of low-O_2 waters. Although, due to the smaller imposed pCO_2 forcing, increases in suboxic volume simulated for the historical period (+ 2 % for 2013) are smaller than that projected for 2100 in variable stoichiometry models (+ 36 – 50 % [32, 33]). Further expansion of suboxic and hypoxic water bodies in response to anthropogenic forcing has

important implications for the global marine nitrogen cycle, with a coeval increase in simulated denitrification rates (34 %; 0 – 2000 m) associated with the elevated consumption of nitrate (NO_3^{2-}) in microbial decomposition of organic material under suboxic conditions. A series of parallel PlankTOM10-NEMOv3.1 sensitivity experiments carried out using a diagnostic N_2O model [73] also indicate that pCO_2-sensitive C:N ratios drive enhanced historical marine N_2O production via promotion of high-yield low-O_2 processes (e.g. denitrification, nitrifier-denitrification).

As noted by [93], however, caution is required when extrapolating the results of mesocosm experiments carried out with one natural plankton assemblage [28] to the global scale for all phytoplankton taxa and biogeographical provinces. Therefore, whilst model parameterisations based around the results of [28] comprise an aggregation of data points across nine large mesocosm enclosures at varying pCO_2, further experimental evidence from diverse marine systems under different environmental conditions is required to better constrain this potentially significant ocean carbon cycle feedback in models. To this end, [94] highlight that, despite good agreement within unialgal cultures towards elevated C:N ratios in response to acidification, reported stoichiometric changes within CO_2 manipulation experiments carried out on natural plankton communities are much more variable. Differences between results are attributed in part to changing experimental practice, such as "batch-mode" versus continuous culture incubation methods. However, a number of external biological factors are also invoked to explain the inconsistent response of natural assemblages to elevated pCO_2, including differing zooplankton grazing rates or community composition between oceanographic regimes. For instance, [95] demonstrate for the Arctic pelagic ecosystem that elemental stoichiometry changes within phytoplankton biomass depend critically on the nature of growth-limiting factors within the heterotrophic community. Additional uncertainties are entrained into biogeochemical model experiments which include variable C:N ratios due to the lack of a process-level understanding for the excess carbon uptake reported by [28] in response to rising pCO_2. For instance, as suggested by [96], additional fixed DIC could be released as Dissolved Organic Carbon (DOC), and contribute to carbon export through the formation of transparent exopolymer particles (TEPs, [97]) via increased aggregation and particle sinking.

Our results also suggest that accounting for pCO_2-driven perturbation to biogenic calcification rates has only a negligible impact on model simulated $[O_2]$ dynamics for the historical period. However, as highlighted by [98] unresolved questions regarding the observed "form and sensitivity" of ocean acidification impacts on calcification introduce uncertainties into the parameterisations adopted in global models such as PlankTOM10. Moreover, the impact of ocean acidification on the "PIC:POC rain ratio" must be considered alongside other external influences on the biological pump, particularly changes in export production in response to ocean warming [88, 6]. For instance, model simulated historical [87] and future [88, 6] reductions in overall export production associated with increased density stratification may act to moderate the impact of any acidification driven reductions in $CaCO_3$ production on EXP_{CaCO3}/EXP_{POC}. Although, whilst this study suggests that pCO_2-calcification effects may be less important for biogeochemical cycles over the historical period, these processes may remain relevant on centennial [38] and millennial [42] timescales.

Finally, our results suggest that imposed atmospheric forcing plays a major role in modulating interannual variability in subsurface $[O_2]$. Particularly, in agreement with forced ocean biogeochemistry model results of [86] for the North Atlantic, simulated interannual variability in $[O_2]$ is shown here to be primarily associated with heat fluxes (σ_θ) in extratropical (mainly subpolar) regions and wind stress (σ_{wspd}) in the tropics. Large uncertainties between prescribed meteorological datasets in these regions propagate into simulated thermocline $[O_2]$, consistent with a recent inter-comparison of surface reanalysis data, which attributes elevated multiproduct inconsistency in the tropics and extratropics chiefly to wind stress and heat flux uncertainties, respectively [99]. The important role of tropical zonal wind stress in controlling variations in model simulated low-O_2 water bodies has been demonstrated in recent work [100, 24] providing further motivation for the provision of appropriate wind forcing to ocean-only models investigating O_2 dynamics.

Whilst all atmospheric forcing products used here provide surface fluxes which are *a priori* representative of observed changes in meteorological variables (aside from *IPSL*), data choices still place major constraints on simulated changes in ocean properties. Further work is required to better understand the biases in atmospheric forcing datasets, both in terms of comparing meteorological fields (e.g. [99]) and assessing how uncertainties in these prescribed forcings (and bulk formulae) impact upon the evolution of hindcast variables. Towards this objective, the Coordinated Ocean-ice Reference Experiments (COREs) project proposes a standard protocol for running hindcast ocean-ice models, emphasising the need for models to be integrated using different atmospheric forcings in order to "assess implications on the ocean and sea ice climate of various atmospheric reanalysis or observational products" [101]. However, the majority of recent physical [102] and biogeochemical [103] multi-model hindcast studies remain focused on investigating the implications of a common atmospheric forcing for a range of ocean models. This approach assumes that all data products provide an equally appropriate representation of historical changes in observed air-sea fluxes. Rather, as argued here, a multifaceted approach is required in order to better evaluate surface meteorological data products, involving both multi-model inter-comparison under a common atmospheric forcing (e.g. COREv2-IAF; [102]) and ensembles of different atmospheric forcing experiments using a common ocean model.

In this study we have presented an analysis of processes using a relatively coarse global ocean biogeochemistry model, which shares some of the shortcomings on the representation of [O_2] as similar models noted in Section 1. To ensure the model shortcomings had a limited effect on the process-based results presented here, we initialized the model with observations and removed the ensuing drift by isolating processes using the *REF* reference simulation. This methodology is unlikely to influence the main conclusions of our analysis on the potential influence of specific processes and the large role of atmospheric forcing for variability, but it could have a larger influence on N_2O fluxes which are more regulated by narrow ranges in low [O_2]. Further work could examine the interactions between physical and biogeochemical factors using a higher-resolution model, particularly to better quantify processes that influence oceanic N_2O emissions.

References

1. Williams J et al. 2014. Numerical simulations of oceanic oxygen cycling in the FAMOUS Earth-System model: FAMOUS-ES, version 1.0. *Geosci. Model Dev* **7**, 1419-1431. (doi:10.5194/gmd-7-149-2014)
2. Keeling R et al. 2010. Ocean deoxygenation in a warming world. *Ann. Rev. Mar. Sci.* **2**, 199-229. (doi:10.1146/annurev.marine.010908.163855)
3. Codispoti L. 2010. Interesting times for marine N_2O. *Science* **327**, 1339-1340
4. Ciais, P et al. 2013. Carbon and Other Biogeochemical Cycles, in Climate Change 2013: The Physical Science Basis. Contribution of Working Group I to the Fifth Assessment Report of the Intergovernmental Panel on Climate Change, edited by: Stocker et al., Cambridge University Press, Cambridge, UK and New York, NY, USA.
5. Doney, S. et al. 2014. Historical and future trends in ocean climate and biogeochemistry, *Oceanography* **2**, 108-119 (http://dx.doi.org/10.5670/oceanog.2014.14)
6. Bopp, L. et al. 2013. Multiple stressors of ocean ecosystems in the 21st century: projections with CMIP5 models, *Biogeosciences* **10**, 6225-6245 (doi:10.5195/bg-10-6225-2013)
7. Cocco, V. et al. 2013. Oxygen and indicators of stress for marine life in multi-model global warming projections, *Biogeosciences* **10**, 1849-1868 (doi:10.5194/bg-10-1849-2013)
8. Andrews, O. et al. 2013. Detecting an external influence on recent changes in oceanic oxygen using an optimal fingerprinting method, *Biogeosciences* **10**, 1799-1813 (doi:10.5194/bg-10-1799-2013)
9. Stramma, L. et al. 2012. Mismatch between observed and modeled trends in dissolved upper-ocean oxygen over the last 50 yr, *Biogeosciences* **9**,4045-4057 (doi:10.5194/bg-9-4045-2012)
10. Duteil, O. et al. 2014. Major role of the equatorial current system in setting oxygen levels in the eastern tropical Atlantic Ocean: A high-resolution model study, *Geophys. Res. Lett.* ***41***, 2033-2040 (doi:10.1002/2013GL058888)
11. Cabré, A. et al. 2015. Oxygen minimum zones in the tropical Pacific across CMIP5 models: mean state differences and climate change trends, *Biogeosciences*, **12** 5429-5454, (doi:10.5194/bg-12-5429-2015)
12. Bopp, L. et al. 2002. Climate-induced oceanic oxygen fluxes: Implications for the contemporary carbon budget, *Glob. Biogeochem. Cy.*, **16** 6225-6245, (doi:10.1029/2001GB001445)
13. Matear, R. and Hirst, A. 2003. Long-term changes in dissolved oxygen concentrations in the ocean caused by protracted global warming, *Glob. Biogeochem. Cy.*, **17** 1125, (doi:10.1029/2002GB001997)
14. Stramma, L. et al. 2008. Expanding oxygen-minimum zones in the tropical oceans, *Science* **320**, 655–658.
15. Gnanadesikan, A. et al. 2013. Critical role for mesoscale eddy diffusion in supplying oxygen to hypoxic ocean waters, *Geophys. Res. Lett.* **40**, 5194–5198, (doi:10.1002/Grl.50998)
16. Bianchi, D. et al. 2012. Data-based estimates of suboxia, denitrification, and N_2O production in the ocean and their sensitivities to dissolved O_2, *Global Biogeochem. Cy.* **26**, (doi:201210.1029/2011GB004209)
17. Jones, C. et al. 2011. The HadGEM2-ES implementation of CMIP5 centennial simulations, Geosci. Model Dev., **4** 543–570, (doi:10.5194/gmd-4-543-2011)
18. Ilyina, T. et al. 2013. The global ocean biogeochemistry model HAMOCC: Model architecture and performance as component of the MPI-Earth System Model in different CMIP5 experimental realizations, *J. Adv. Model. Earth. Sy.*, **5** 287-315, (doi:10.1002/jame.20017)
19. Dunne, J. et al. 2013. GFDL's ESM2 global coupled climate-carbon Earth System Models Part II: carbon system formulation and baseline simulation characteristics, *J. Climate*, (doi:10.1175/JCLI-D-12-00150.1)
20. Brandt, P. et al. 2010. Changes in the Ventilation of the Oxygen Minimum Zone of the Tropical North Atlantic, *J. Phys. Oceanogr.*, **40**, 1784–1801, (doi:http://dx.doi.org/10.1175/2010JPO4301.1)

21. Resplandy, L. et al. 2012. Controlling factors of the oxygen balance in the Arabian Sea's OMZ, *Biogeosciences* **9**, 5095-5109, (doi:10.5194/bg-9-5095-2012)
22. Gnanadesikan, A. et al. 2012. Understanding why the volume of suboxic waters does not increase over centuries of global warming in an Earth System Model, *Biogeosciences* **9**, 1159–1172, (doi:10.5194/bg-9-1159-2012)
23. Duteil and Oschlies. 2011. Sensitivity of simulated extent and future evolution of marine suboxia to mixing intensity, *Geophys. Res. Lett.* **38**, L06607, (doi:10.1029/2011GL046877)
24. Deutsch, C. et al. 2014. Centennial changes in North Pacific anoxia linked to tropical trade winds, *Science* **345** 665, (doi:10.1126/science.1252332)
25. McKinley, G. et al. 2003. Interannual variability of air-sea O_2 fluxes and the determination of CO_2 sinks using atmospheric O_2/N_2, *Geophys. Res. Lett.* **30**, 1101, (doi:10.1029/2002GL016044)
26. Rödenbeck, C. et al. 2008. Interannual variability in oceanic biogeochemical processes inferred by inversion of atmospheric O2/N2 and CO2 data, *Tellus B – Chem. Phys. Meteorol.*, 60, 685–705.
27. Matear, R and Lenton, A. 2014. Quantifying the impact of ocean acidification on our future climate, *Biogeosciences* **11**, 3965-3983, (doi:10.5194/bg-11-3965-2014)
28. Riebesell , U. et al. 2007. Enhanced biological carbon consumption in high CO_2 ocean, *Nature* **450**, 545–548.
29. Bellerby, R. et al. 2008. Marine ecosystem community carbon and nutrient uptake stoichiometry under varying ocean acidification during the PeECE III experiment, *Biogeosciences* **5**, 1517-1527, (doi:10.5194/bg-5-1517-2008)
30. Redfield, A. et al. 1963. The influence of organisms on the composition of sea-water, in: The sea, edited by: Hill, M. N., New York, Wiley, 2, 26–77.
31. Flynn, J. Ecological modelling in a sea of variable stoichiometry: Dysfunctionality and the legacy of Redfield and Monod, *Prog. Oceanog.*, **84**, 52–65.
32. Oschlies, A. et al. 2008. Simulated 21st century's increase in oceanic suboxia by CO_2-enhanced biotic carbon export, *Global. Biogeochem. Cy.*, **22**, GB4008, (doi:10.1029/2007GB003147)
33. Tagliabue, A. et al. 2011. The response of marine carbon and nutrient cycles to ocean acidification: Large uncertainties related to phytoplankton physiological assumptions, *Global Biogeochem. Cy.*, **25**, GB3017, (doi:10.1029/2010GB003929)
34. Buitenhuis, E. et al. 2013. Combined constraints on global ocean primary production using observations and models, *Global Biogeochem. Cy.*, **27**, 847–858, (doi:10.1002/gbc.20074)
35. Le Quéré, C. et al. 2016. Role of zooplankton dynamics for Southern Ocean phytoplankton biomass and global biogeochemical cycles, *Biogeosciences* **13**, 4111-4133, (doi:10.5194/bg-13-4111-2016)
36. Feely, R. et al. 2004. Impact of Anthropogenic CO_2 on the $CaCO_3$ System in the Oceans, *Science* **305**, 362 – 366, (doi: 10.1126/science.1097329)
37. Fabry, W. et al. 2008. Impacts of ocean acidification on marine fauna and ecosystem processes, *ICES J. Mar. Sci.* ***65***, 414-432 (doi:10.1093/icesjms/fsn048)
38. Heinze, C. 2004. Simulating oceanic CaCO3 export production in the greenhouse, *Geophys. Res. Lett.*, **13**, L16308, doi:10.1029/2004GL020613, 2004.
39. Armstrong, R. et al. 2002. A new, mechanistic model for organic carbon fluxes in the ocean: based on the quantitative association of POC with ballast minerals, *Deep-Sea Res. II*, **49**, 219–236
40. Archer, D. et al. 2000. What caused the glacial/interglacial atmospheric pCO_2 cycles?, *Rev. Geophys.*, **38**, 159-189.
41. Klass, C. and Archer, D. 2002. Association of sinking organic matter with various types of mineral ballast in the deep sea: Implications for the rain ratio, *Global Biogeochem. Cy.*, **16**, 1116.
42. Hofmann, M. and Schellenhuber, H. 2009. Ocean acidification affects marine carbon and triggers extended marine oxygen holes, *Proc. Natl. Acad. Sci.*, **106**, 3017-2033.
43. Deutsch, C. et al. 2005. Fingerprints of climate change in North Pacific oxygen, *Geophys. Res. Lett.*, **32**, L16604, (doi:10.1029/2005GL023190)
44. Deutsch, C. et al. 2006. Physical-biological interactions in North Pacific oxygen variability, *J. Geophys. Res.*, **111**, C09S90, (doi:10.1029/2005JC003179)
45. Swart, N. et al. 2014. Wind driven changes in the ocean carbon sink, *Biogeosciences Discuss.*, **11**, 8023-8048, (doi:10.5194/bgd-11-8023-2014).
46. Le Quéré, C. et al. 2010. Impact of climate change and variability on the global oceanic sink of CO2, *Global Biogeochem. Cy.*, **24**, GB4007, (doi:10.1016/0012-821X(72)90242-7)
47. Ishi, M. et al. 2014. Air–sea CO2 flux in the Pacific Ocean for the period 1990–2009, *Biogeosciences*, **11**, 709-734, (doi:10.5194/bg-11-709-2014)
48. Atlas, R. et al. 2011. A cross calibrated multiplatform ocean surface wind velocity product for meteorological and oceanographic applications, *B. Am. Meteor. Soc.* **92**, 157- 174
49. Kalnay, E. et al. 1996. The NCEP/NCAR 40-year reanalysis project, *B. Am. Meteor. Soc.* **77**, 437–471, 1996
50. Stepanov, V. and Haines, K. 2014. Mechanisms of Atlantic Meridional Overturning Circulation variability simulated by the NEMO model, *Ocean Sci.* **10**, 645-656, (doi:10.5194/os-10-645-2014)
51. Simmons, A. et al. ERA-Interim: New ECMWF reanalysis products from 1989 onwards. Newsletter 110 - Winter 2006/07, ECMWF, 11.
52. Brodeau, L., et al. 2010. An ERA 40 based atmospheric forcing for global ocean circulation models, *Ocean Modell.* **31**, 88–104.
53. Large, W. and Yeager, S. Diurnal to decadal global forcing for ocean and sea-ice models: the datasets and flux climatologies, Tech. Rep. TN-460+STR, NCAR, Boulder, Colorado.
54. Le Quéré, C. et al. 2005. Ecosystem dynamics based on plankton functional types for global ocean biogeochemistry models, *Glob. Change Biol.* **11**, 2016–2040, (doi:10.1111/j.1365-2486.2005.1004.x)
55. Buitenhuis, E. et al. 2010. Biogeochemical fluxes through microzooplankton, *Global Biogeochem. Cy.* **24**, GB4015, (doi:10.1029/2009GB003601)
56. Takahashi, T., et al.: 1985. Redfield ratio based on chemical data from isopycnal surfaces, *J. Geophys. Res.*, **90**, 6907–6924.
57. Ploug, H. et al. 2008. Production, oxygen respiration rates, and sinking velocity of copepod fecal pellets: Direct measurements of ballasting by opal and calcite, *Limnol. Oceanogr* **53**, 469–476.
58. Buitenhuis, E. et al. 2001. Blooms of Emiliania huxleyi are sinks of atmospheric carbon dioxide: A field and mesocosm study derived simulation, *Global Biogeochem. Cy.*, **15**, 577–587, (doi:10.1029/2000GB001292)
59. Key, R. et al. 2004. A global ocean carbon climatology: Results from Global Data Analysis Project (GLODAP), *Global Biogeochem. Cy.*, **18**, GB4031, (doi:10.1029/2004GB002247)
60. Garcia, H. et al. 2006. World Ocean Atlas 2005, Volume 3: Dissolved Oxygen, Apparent Oxygen Utilization, and Oxygen Saturation, in: *World Ocean Atlas 2005*, edited by: Levitus, S., NOAA Atlas NESDIS 62, US Government Printing Office, Washington, DC.
61. Garcia, H. et al. 2006. World Ocean Atlas 2005, Volume 4: Nutrients (phosphate, nitrate, silicate), in: *World Ocean Atlas 2005*, edited by Levitus, S., NOAA Atlas NESDIS 64, US Government Printing Office, Washington, DC, pp. 396
62. Vogt, M. et al. 2010. Simulating dimethylsulphide seasonality with the Dynamic Green Ocean Model PlankTOM5, *J. Geophys. Res.*, **115**, C06021, (doi:10.1029/2009JC005529)
63. Keeling, C and Whorf, T. 2005. Atmospheric CO_2 records from sites in the SIO air sampling network, In *Trends: A Compendium of Data on Global Change*. Carbon Dioxide Information Analysis Center, Oak Ridge National Laboratory, U.S. Department of Energy, Oak Ridge, Tenn., USA,
64. Jickells, T. et al. 2005. Global iron connections between desert dust, ocean biogeochemistry, and climate, *Science*, **308**, 67–71, 2005
65. Madec, G. 2008. NEMO ocean engine, Note du Pole de modelisation, Institut Pierre-Simon Laplace (IPSL), Paris, No 27.
66. Timmermann, R. et al. 2006. On the representation of high latitude processes in the ORCA-LIM global coupled sea ice–ocean model, *Ocean Model.* **8**, 175–201, (doi:10.1016/j.ocemod.2003.12.009)
67. Madec, G. and Imbard, M. 1996. A global ocean mesh to overcome the North Pole singularity, *Clim. Dynam.* **12**, 381–388
68. Gaspar, P. et al. 1990. A simple eddy kinetic energy model for simulations of the oceanic vertical mixing tests at station papa and long–term upper ocean study site, *J. Geophys. Res.* **95**, 16179–16193
69. Gent, P. and McWilliams, J. 1990. Isopycnal mixing in ocean circulation models, *J. of Phys. Oceanog.*, **20**, 1–6
70. Antonov, J. et al. 2006. *World Ocean Atlas 2005*, Vol. 2: Salinity, edited by: Levitus, S.,. NOAA Atlas NESDIS 62 US Government Printing Office, Washington, DC, 182 pp.
71. Locarnini, R. et al. 2006. *World Ocean Atlas 2005*, Vol. 1: Temperature, edited by: Levitus, S., NOAA Atlas NESDIS 61, US Government Printing Office, Washington, DC, 182 pp., 2006
72. Manizza, M. et al. 2008. Ocean biogeochemical response to phytoplankton-light feedback in a global model, *J. Geophys. Res.-Oceans* **113**, C10010, (doi:10.1029/2007JC004478)
73. Suntharalingam, P. et al. 2012. Quantifying the Impact of Anthropogenic Nitrogen Deposition on Oceanic Nitrous Oxide, *Geophys. Res. Lett.* **39**, L07605, (doi:10.1029/2011GL050778)
74. Zondervan, I. et al. 2001. Decreasing marine biogenic calcification: A negative feedback on rising atmospheric pCO2, *Global Biogeochem. Cy.* **15**, 507–516
75. Goosse, H. et al. 1999. Sensitivity of a global coupled ocean-sea ice model to the parameterization of vertical mixing, *J. Geophys. Res.* **104**, 13681–13695
76. Large, W. and Yeager, S. 2009. The global climatology of an interanually varying air-sea flux dataset, *Clim. Dynam.* **33**, 341–364
77. Zhang, Y. et al. 2004. Calculation of radiative fluxes from the surface to top-of-atmosphere based on ISCCP and other global datasets: Refinements of the radiative transfer model and the input data, *J. Geophys. Res.* **109**, D19105, (doi:10.1029/2003JD004457)
78. Uppala, S. et al. 2005. The ERA-40 re-analysis, *Q. J. R. Meteorol. Soc.* **131**, 2961–3012
79. Séférian et al. 2013. Skill Assessment of Three Earth System Models with Common Marine Biogeochemistry, *Clim. Dynam.* **40**, 9–10, (doi:10.1007/s00382-012-1362-8)
80. Taylor, K. et al. 2012. An overview of CMIP5 and the Experiment Design, *Bull. Amer. Meteor. Soc.*, **93**, 485–498, (doi:10.1175/BAMS-D-11-00094.1)

81. Yool, A. et al. 2013. Climate change and ocean acidification impacts on lower trophic levels and the export of organic carbon to the deep ocean, *Biogeosciences* **10**, 5831–5854, (doi:10.5194/bg-10-5831-2013)
82. Whitney, F. et al. 2013. Nutrient enrichment of the subarctic Pacific Ocean pycnocline, *Geophys. Res. Lett.,* **40**, 2200 – 2205, (doi:10.1002/grl.50439)
83. Whitney, F. et al. 2007. Persistently declining oxygen levels in the interior waters of the eastern subarctic Pacic, *Prog. Oceanogr.* **75**, 179–199
84. Sydeman, W. et al. 2011. Does positioning of the North Pacific Current affect downstream ecosystem productivity?, *Geophys. Res. Lett.* **38**, L12606, (doi:10.1029/2011GL047212)
85. Frölicher, T. et al. 2009. Natural variability and anthropogenic trends in oceanic oxygen in a coupled carbon-climate model ensemble, *Global Biogeochem. Cy.* **23**, GB1003, (doi:10.1029/2008GB003316)
86. Freidrich, T. et al. 2006. Role of wind stress and heat fluxes in interannual-to-decadal variability of air-sea CO_2 and O_2 fluxes in the North Atlantic, *Geophys. Res. Lett.* **33**, L21S04, (doi:10.1029/2006GL026538)
87. Laufkötter, C. et al. 2013. Long-term trends in ocean plankton production and particle export between 1960–2006, *Biogeosciences* **10**, 7373-7393, (doi:10.5194/bg 10-7373-2013)
88. Steinacher, M. et al. 2010. Projected 21st century decrease in marine productivity: a multi-model analysis, *Biogeosciences* **7**, 979-1005, (doi:10.5194/bg-7-979-2010)
89. Boyce, D. et al. 2010. Global phytoplankton decline over the past century, *Nature*, **466**, 591–596, (doi:10.1038/nature09268)
90. Rykaczewski, R. and Dunne, J. 2011. A measured look at ocean chlorophyll trends, *Nature*, **472**, E5–E6, (doi:10.1038/nature09952)
91. Butenschön, M., et al. 2016. ERSEM 15.06: a generic model for marine biogeochemistry and the ecosystem dynamics of the lower trophic levels, *Geosci. Model Dev.*, **9**, 1293-1339, (doi:10.5194/gmd-9-1293-2016).
92. Helm, K. et al. 2011. Observed decreases in oxygen content of the global ocean, *Geophys. Res. Lett.* **38**, L23602, (doi:10.1029/2011GL049513)
93. Matear, R. and McNeil, B. 2009. Enhanced biological carbon consumption in a high CO_2 ocean: a revised estimate of the atmospheric uptake efficiency, *Biogeosciences Discuss.* **6**, 8101-8128, (doi:10.5194/bgd-6-8101-2009)
94. Hutchins, D. et al. 2009. Nutrient cycles and marine microbes in a CO_2-enriched ocean, *Oceanography* **22**, 128–145
95. Thingstad, T. et al. 2008. Counterintuitive carbon-to-nutrient coupling in an Arctic pelagic ecosystem, *Nature* **455**, 387–390, (doi:10.1038/Nature07235)
96. Arrigo, K. R., 2007. Carbon cycle: Marine manipulations, *Nature*, **450**, 491–492.
97. Engel, A., 2002. Direct relationship between CO_2 uptake and transparent exopolymer particles in natural phytoplankton, *J. Plankton Res.*, **24**, 49–53, doi:10.1093/plankt/24.1.49.
98. Ridgwell, A. et al. 2009. From laboratory manipulations to Earth system models: scaling calcification impacts of ocean acidification, *Biogeosciences* **6**, 2611-2623, (doi:10.5194/bg-6-2611-2009)
99. Chaudhuri, A. et al. 2013. A comparison of atmospheric reanalysis surface products over the ocean and implications for uncertainties in air–sea boundary forcing, *J. Clim.* **26**, 153–170. (doi:http://dx.doi.org/10.1175/JCLID-12-00090.1)
100. Ridder, N. and England, E. 2014. Sensitivity of ocean oxygenation to variations in tropical zonal wind stress magnitude, *Global Biogeochem. Cy.* **28**, (doi:10.1002/2013GB004708)
101. Griffies, S. et al. Coordinated ocean-ice reference experiments (COREs), *Ocean Model.* **26**, 1–46
102. Danabasoglu, G. et al. North Atlantic simulations in coordinated ocean-ice reference experiments phase II (CORE-II), Part I: Mean states, *Ocean Model.* **73**, 76–107, (doi:10.1016/j.ocemod.2013.10.005)
103. Kwiatkowski, L. et al. 2014. iMarNet: an ocean biogeochemistry model inter-comparison project within a common physical ocean modeling framework, *Biogeosciences Discuss.* **11**, 10537-10569, (doi:10.5194/bgd-11-10537-2014)

Additional information

Acknowledgments

We thank C. Enright for programming support. Model experiments and analyses presented in this paper were carried out on the High Performance Computing Cluster supported by the Research and Specialist Computing Support service at the University of East Anglia. We acknowledge the World Climate Research Programme's Working Group on Coupled Modelling, which is responsible for CMIP, and we thank the climate modelling groups for producing and making available their model output. For CMIP the U.S. Department of Energy's Program for Climate Model Diagnosis and Intercomparison provides coordinating support and led development of software infrastructure in partnership with the Global Organization for Earth System Science Portals.

Funding Statement

This work was supported by the European Union's Horizon 2020 research and innovation programme under grant agreement no. 641816 (CRESCENDO).

Data Accessibility

Model data can be made available by contacting O.A. Model restart files are available at http://opendap.uea.ac.uk:8080/opendap/greenocean/Restart. Forcing and CMIP5 data used in this study are publically available.

Competing Interests

The authors declare that they have no competing interests.

Authors' Contributions

Conception and design of the study by all authors. Model development and testing by E.B., C.L.Q. and O.A. Model runs, analysis and first manuscript draft by O.A. All authors contributed to the interpretation of results and drafting of the final manuscript.

Figures

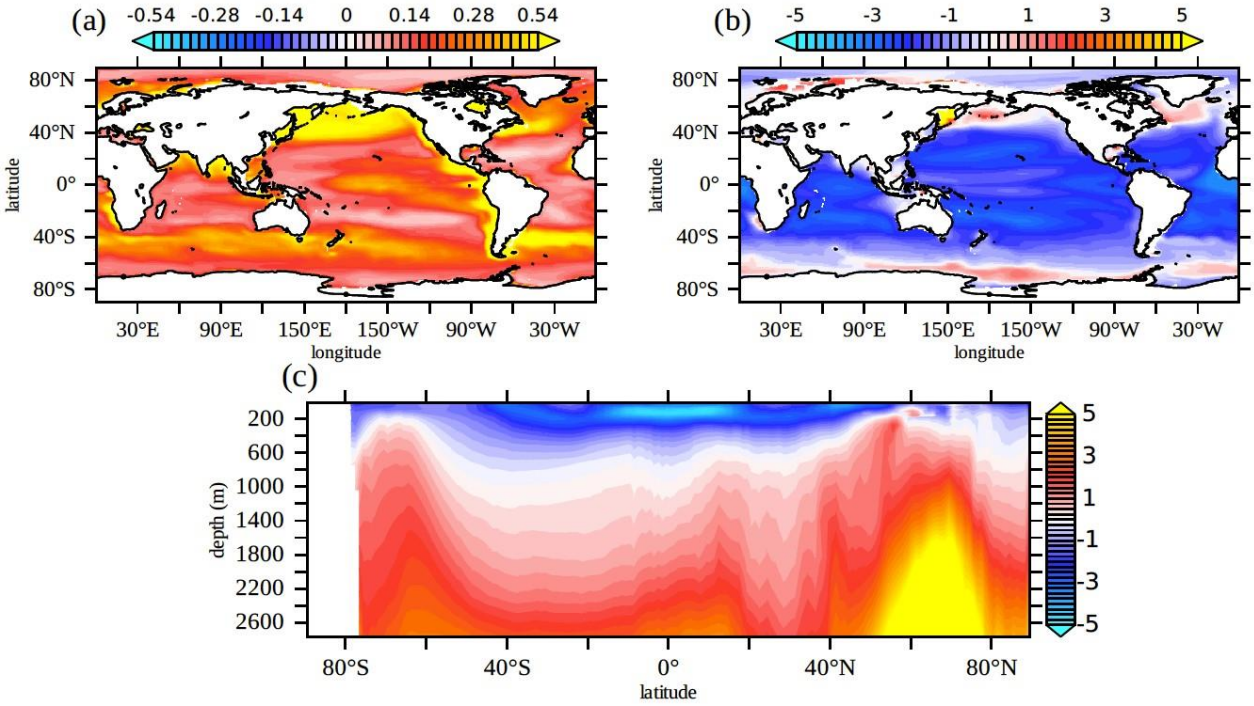

Fig. 1. Differences in modelled ocean carbon cycle variables (*STO10* simulation minus *REF*) averaged over 2003 – 2013. (**A**) POC export (mol C m^{-2} y^{-1}) at 100 m depth, (**B**) Concentration of DIC (µmol L^{-1}) at 100 m depth, (**C**) zonal mean DIC concentration.

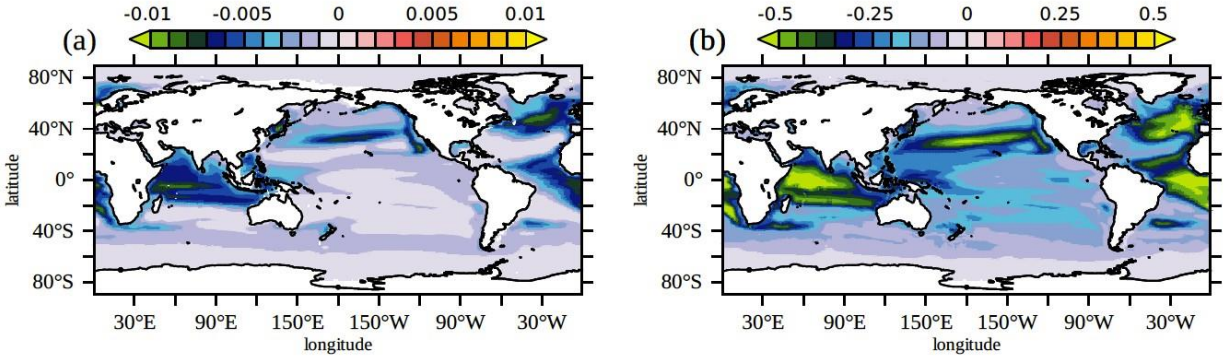

Fig. 2. Differences in modelled ocean carbon cycle variables (*BAL10* simulation minus *REF*) averaged over 2003 – 2013. (**A**) EXP_{CaCO3}/EXP_{POC} at 100 m depth and (**B**) gravitational sinking speeds for large POC *vsink* (m d^{-1}) between 0 - 2000 m.

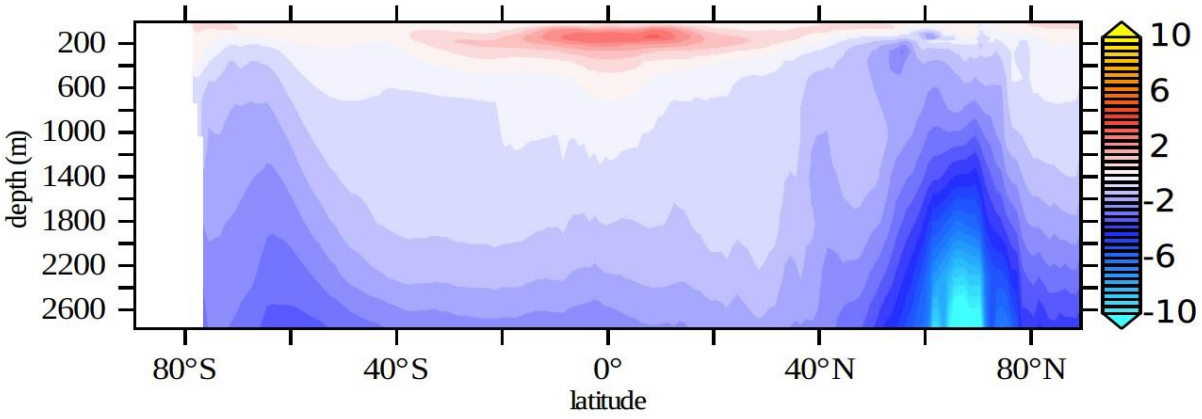

Fig. 3. Difference in modelled zonal mean [O_2] (μmol L^{-1}) compared with simulation *REF* for (**A**) *STO10*, (**B**) *BAL10* averaged over 2003 – 2013 (blue colours indicate historical deoxygenation relative to *REF)*.

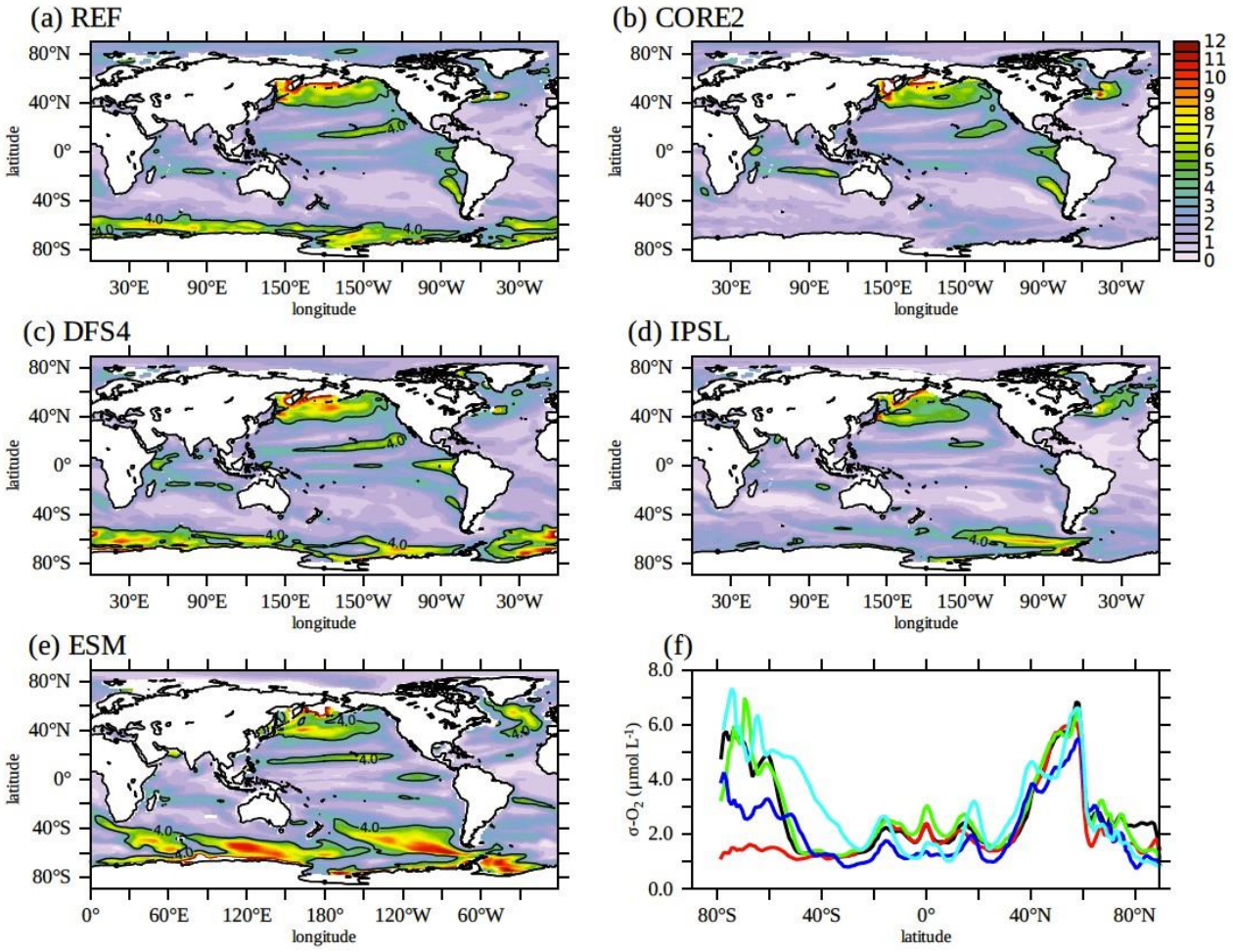

Fig. 4. Interannual variability (σ) in modelled annual mean [O_2] (μmol L^{-1}) at 300 m depth for a range of model experiments. (**A**) *REF* (black in Panel F), (**B**) *CORE2* (red), (**C**) *DFS4* (green), (**D**) *IPSL* (blue) and (**E**) ESM (turquoise). [O_2] contours are overlain in black for $\sigma_{[O2]} = 4$ μmol L^{-1}. Zonal mean inter-annual variability in [O_2] at 300 m for all model experiments is presented in Panel **F**. A boxcar (low-pass) filter is applied in order to diagnose secular trends in subsurface [O_2], with the 10-year running mean being removed at each grid point in order to retain only an estimate of inter-annual (unforced) variability. The interannual variability is computed over the 1958 – 2005 time period, common to all forcing products.

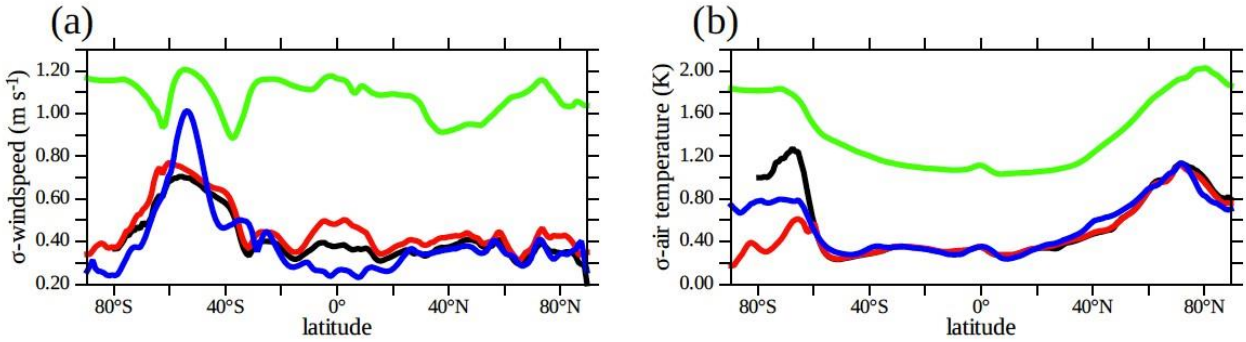

Fig. 5. Interannual variability (σ) in de-trended zonal mean (**A**) windspeed (m s^{-1}) and (**B**) near-surface air temperature (θ; K) for NCEP/NCAR reanalysis (black), COREv2-IAF (red) and DFS4.3 (green) products, and IPSL-CM5A-LR derived atmospheric fields (blue). Following [45] windspeed is plotted as a measure of momentum flux rather than wind stress since the latter has a strong dependency on the choice of drag coefficient.

Tables

Table 1. Summary of the model configurations used in each ocean-only model experiment.

Model experiment	Time period	Atmospheric Forcing	pCO_2-sensitive C:N ratio	pCO_2-sensitive R_{CAL}
REF	1948 - 2013	NCEP/NCAR	No	No
STO10	1948 - 2013	NCEP/NCAR	Yes	No
BAL10	1948 - 2013	NCEP/NCAR	No	Yes
CORE2	1948 - 2007	COREv2-IAF	No	No
DFS4	1958 - 2006	DFS4.3	No	No
IPSL	1948 - 2005	IPSL-CM5A-LR	No	No

Table 2. Summary of atmospheric forcing datasets used in model experiments. The temporal frequency of meteorological surface variables is provided in parentheses (*di* = 6 hourly [diurnal]; *d* = daily, *m* = monthly).

EXP	Dataset	Time period	Bulk formulation	U_{10}, V_{10}, θ, q	rad_{sw}, rad_{lw}	*precip*, *snow*
REF[1]	NCEP/NCAR	1948 - 2013	CLIO	NCEP/NCAR (*d*)	N/A[2]	NCEP/NCAR (*d*)[6]
CORE2	COREv2-IAF	1948 - 2007	CORE	NCEP/NCAR[3] (*di*)	ISCCP-FD[3, 5](*d*)	GCGCS[7] (*m*)
DFS4	DFS4.3	1958 - 2006	CORE	ERA-40[4] (*di*)	ISCCP-FD[4, 5] (*d*)	GCGCS[7] (*m*)
IPSL	IPSL-CM5A-LR	1948 - 2005	CORE	CMIP5 (*d*)	CMIP5 (*d*)	CMIP5 (*m*)

[1] The baseline *REF* atmospheric forcing configuration is used for all ocean biogeochemistry experiments
[2] Radiative fluxes calculated from total cloud cover (*tcdc*) following [49]
[3] Bias corrections applied as described in [53, 76]
[4] Bias corrections applied as described in [52]
[5] Forcing provided as a climatological mean annual cycle for prior to 1984
[6] Total precipitation rate used without solid fraction (*snow*)
[7] Forcing provided as a climatological mean annual cycle for prior to 1979

Supplementary material for Andrews, O., Buitenhuis, E., Le Quéré, C., and Suntharalingam, P., 2017, Biogeochemical modelling of dissolved oxygen in a changing ocean, *Phil. Trans. R. Soc. A.* doi: 10.1098/rsta.2016.0328

Supplementary Material

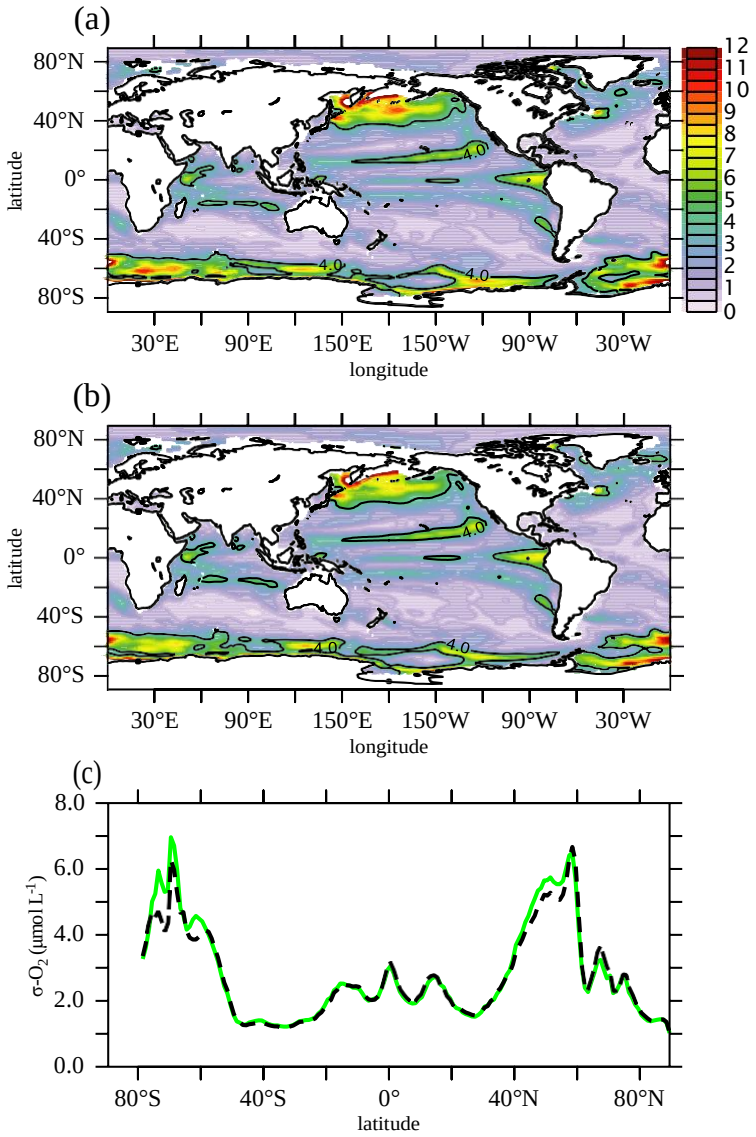

Fig. S1. Interannual variability (σ) in modeled annual mean [O_2] (μmol L^{-1}) at 300 m depth for (**A**) *DFS4* (green), (**B**) *DFS4* (dotted black) using daily frequency input atmospheric forcing for U_{10}, V_{10}, θ and q. Expressed as zonal mean $\sigma_{[O2]}$ at 300 m in panel (**C**).